LA-UR-22-20314

Approved for public release; distribution is unlimited.

Title:	Light-Level Geolocation of the LANL Population of Western Bluebirds
Author(s):	Gadek, Chauncey Ryland Hathcock, Charles Dean
Intended for:	Report
Issued:	2022-01-13

January 2022

Light-Level Geolocation of the LANL Population of Western Bluebirds

Authors: Chauncey R. Gadek and Charles D. Hathcock

Los Alamos NATIONAL LABORATORY

Prepared for:	U.S. Department of Energy/National Nuclear Security Administration, Los Alamos Field Office
Prepared by:	Chauncey R. Gadek, Biologist Charles D. Hathcock, Biologist EPC-ES
Editing and Layout by:	Tamara Hawman, Communications Specialist CEA-CAS
Cover Photo:	Male Western Bluebird (*Sialia mexicana*) fitted with a geolocator

CONTENTS

Figures

Contents

Contents

Tables

1 INTRODUCTION

1.1 Impetus for Study

Options for tracking and reconstructing animal movement are increasingly accessible due to rapidly decreasing costs, smaller sizes, and a proliferation of analytical inference techniques (Rutz and Hays, 2009; Wikelski et al., 2007). A wide variety of options exists for determining movement patterns of animals—from high-resolution pinpoint ARGOS satellite tags to time-consuming and logistically challenging radio telemetry. One option, light-level geolocation, offers small, affordable devices with long battery lives known as global location sensors (GLS), making them ideal for gathering preliminary migratory data. Geolocation works by inferring patterns of animal movement from light-level transitions between day and night (Hill and Braun, 2001).

The recent advances in tracking technologies allow biologists to zoom in on migratory behavior, delineating heretofore-unidentified intraspecific migratory behavior (Delmore et al., 2012). The ubiquity of migratory divides (populations within a species that exhibit different migratory patterns) remains largely unknown, but their existence can lead to favorable demographic metrics (e.g., genetic diversity) in conservation contexts (Møller et al., 2011) and necessitate the development of population-specific conservation plans (Delmore et al., 2012). Delimiting the populations within a species that migrate and the extent of their migrations relative to individuals that remain resident across a species' range has important evolutionary, ecological, and conservation implications. Within this context, Los Alamos National Laboratory (LANL) biologists have leveraged the local Avian Nestbox Network (ANN; Fair and Myers, 2002) to evaluate the migratory behaviors of a common local bird species, the Western Bluebird *(Sialia mexicana)*.

1.2 Western Bluebird Background

The Western Bluebird (WEBL) is a small thrush from the family Turdidae. WEBLs are secondary cavity nesting insectivores and are facultatively omnivorous (AAB, 2019a). The species tends to nest and forage in open woodlands and edge habitats throughout much of the western United States (AAB, 2019b).

Occurrence records and field guides suggest that the WEBL species is comprised of both partial migrants—with populations at the northernmost edge of their range in the Pacific Northwest, Colorado, and northern New Mexico undertaking moderate-distance migrations—and short-distance, elevational migrants in mountainous parts of the species' range (Guinan et al., 2008). The population of WEBLs at

Introduction

LANL resides both near the putative boundary of migratory and sedentary populations (Figure 1-1) and at a moderate elevation implying the potential for both moderate distance migration and short distance elevational migration within the local population (AAB, 2019b).

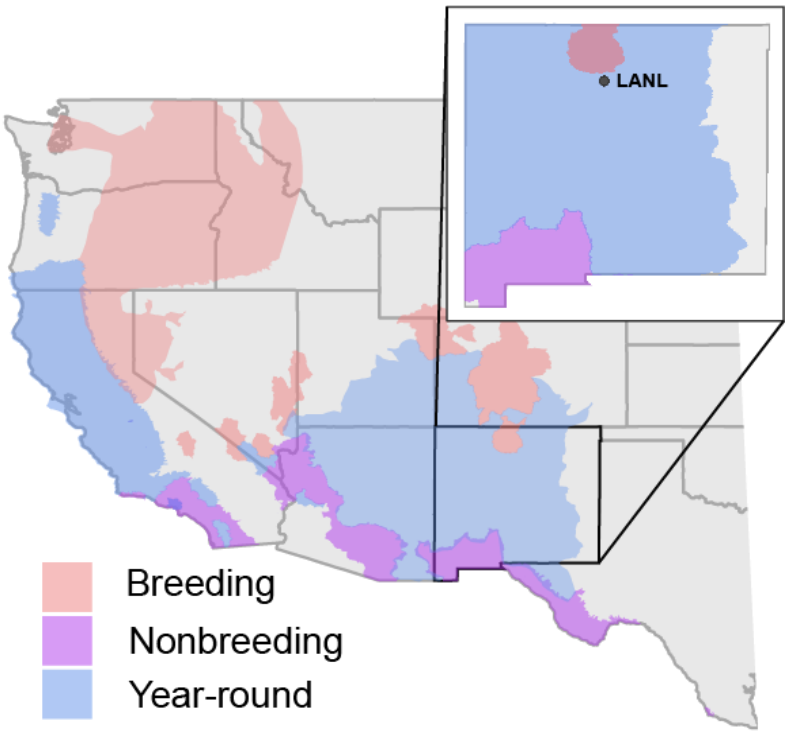

Figure 1-1. Map of United States WEBL range from United States Geological Survey data modified with birds of the world range map with inset showing LANL's position between putatively migratory and resident populations.

The LANL ANN has been collecting data on the Los Alamos County WEBL population since 1997 (Fair and Myers, 2002). The nestbox data have captured upward elevational shifts in occupancy (Wysner et al., 2019) likely due to population-level emigration and immigration processes (Abeyta et al., 2021), but the extent of migratory behavior in local populations of this species remains unknown. Countering expectations of a migratory population, Los Alamos County observations from eBird (eBird, 2021) show no clear pattern in monthly average observations of individual WEBLs between 2008 and 2021 (Figure 1-2). LANL breeding and winter bird survey data (unpublished data) suggest differential habitat utilization between breeding and wintering bluebirds, with breeding birds more often recorded in ponderosa pine habitat and wintering birds more often recorded in pinyon-juniper and riparian/wetland habitat (Figure 1-3). Understanding the migratory status of the LANL population of WEBLs will help LANL biologists

refine migratory bird management practices and build on a 20 plus–year dataset of population demography at LANL that continues to contribute to the field of avian ecology more broadly.

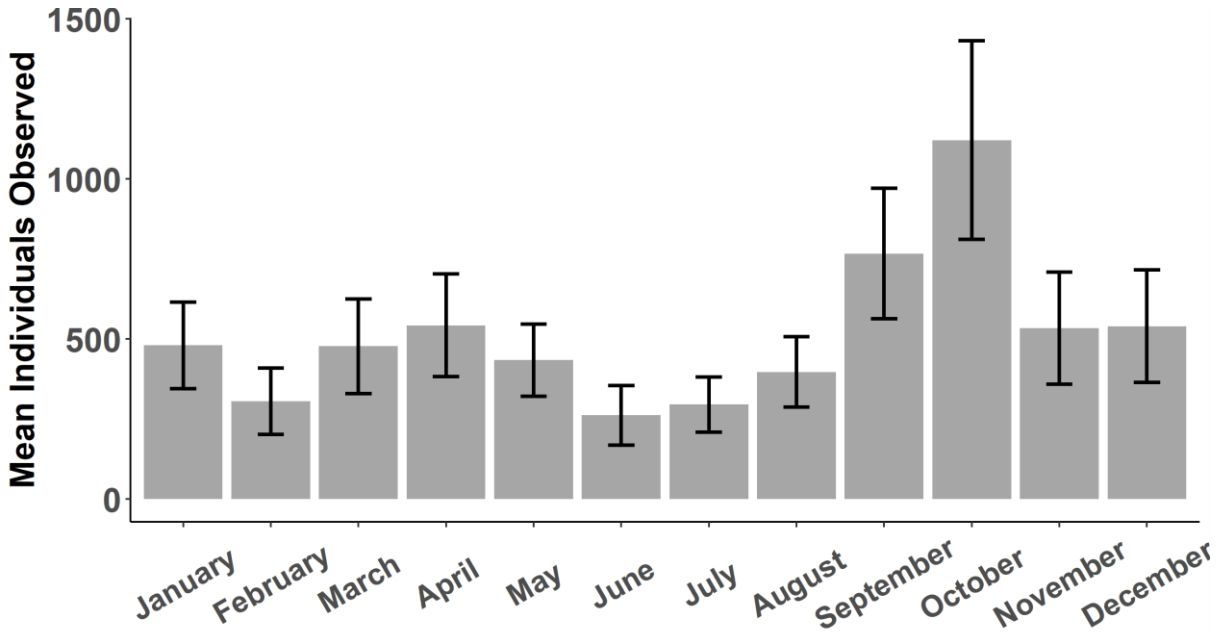

Figure 1-2. Histogram of mean number of individual WEBLs recorded on eBird each month between 2008 and 2021 in Los Alamos County. Black bars show standard error of records. Note the relatively flat trend, with increased reports in September and October.

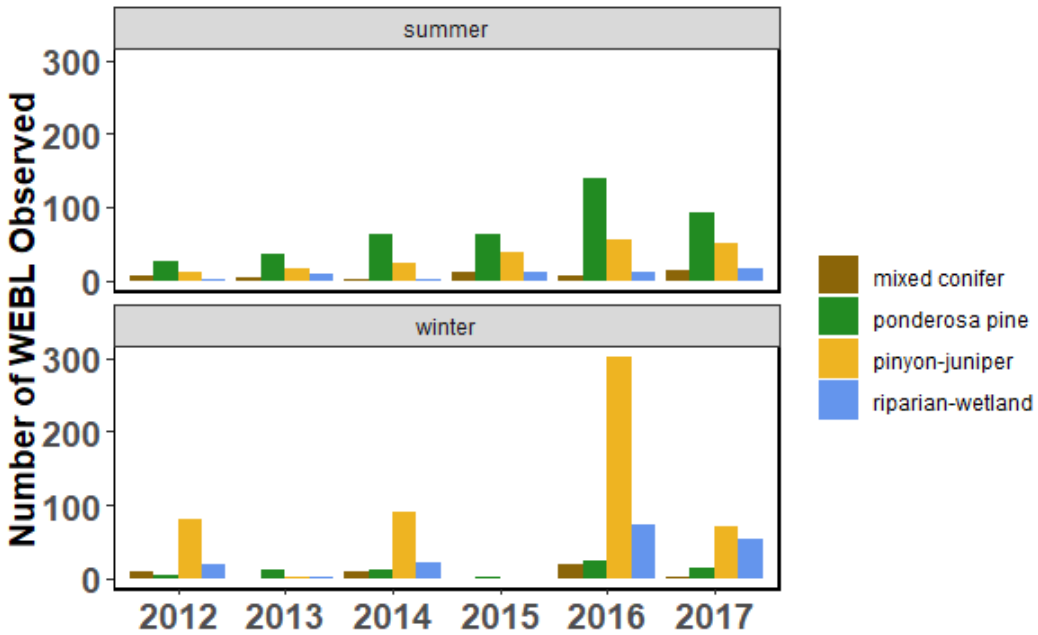

Figure 1-3. Breeding and winter bird survey observations colored by habitat type at LANL and surrounding areas. Notice WEBLs are recorded in ponderosa pine–dominant habitats in the summer versus pinyon-juniper-dominant habitats in the winter.

2 MIGRATORY BEHAVIOR ASSESSMENT METHODS

To initially assess migratory behaviors in local WEBLs, we deployed 44 ML6540 light-level GLSs between May and June 2015 at sites that span the ANN (Table 2-1). Three units were "rooftop" calibrated (Lisovski et al., 2020) by setting activated devices in full sun for about 2 weeks before deployment. We used mist nets to capture adult breeding WEBLs at occupied nestboxes on LANL property and at other sites in Los Alamos County. All animal handling was completed following Institutional Animal Care and Use Committee (IACUC) Protocol 14-60. We secured GLS units using the basic harness design of Rappole and Tipton (1991) as modified in Streby et al. (2015). Before attaching a harness, we measured the bird's mass and determined age and sex by plumage. Immediately after securing the harness to the bird, we logged deployment time and location and observed the bird for a few minutes to ensure that the bird did not exhibit any flight complications from the harness and tag. We recovered tagged birds by hand and with mist nets at nestboxes the following year.

Table 2-1. Summary table of 44 GLSs deployed in 2015. This table gives location, band number, mass (g) at deployment, age at deployment (SY = second year; ASY = after second year), and sex (M = male; F = female) of individual tagged birds. The light blue–shaded portion of table shows individuals from which tags were recovered. Red-shaded rows indicate individual tags recovered from dead birds that died from causes unrelated to the geolocation study and were recovered.

Deployment Date	Location	Band	Mass	Age	Sex
11-Jun-15	Anchor Ranch	2711-62763	25.6	SY	M
28-May-15	Sandia	2711-62705	28.2	ASY	F
26-Jun-15	Ski Hill	2711-62803	23.4	SY	F
19-Jun-15	Anchor Ranch	2711-62797	23.3	ASY	M
26-Jun-15	Ski Hill	2711-62804	25	ASY	F
17-Jun-15	Anchor Ranch	2691-24166	23.4	SY	F
11-Jun-15	Anchor Ranch	2691-24310	24.3	ASY	F
9-Jun-15	Anchor Ranch	2711-62733	25.9	ASY	M
9-Jun-15	Golf Course	2711-62732	27.4	ASY	M
5-Jun-15	Golf Course	2711-62728	27.7	ASY	M
22-May-15	Golf Course	2711-62703	29.8	ASY	F
17-Jun-15	Anchor Ranch	2711-62779	29	ASY	F
1-Jun-15	Cañada del Buey	2711-62712	27	SY	M
1-Jun-15	Cañada del Buey	2711-62711	26.1	SY	F
11-Jun-15	Anchor Ranch	2711-62762	23.7	ASY	M
28-May-15	Golf Course	2711-62706	32.9	ASY	F
19-May-15	Delta Prime Canyon	2711-62702	25.3	ASY	M
28-May-15	Sandia	2711-62704	24.7	ASY	M

Deployment Date	Location	Band	Mass	Age	Sex
28-May-15	Golf Course	2441-18464	24.3	ASY	M
28-May-15	Golf Course	2441-18423	28.2	ASY	F
1-Jun-15	Delta Prime Canyon	2711-62708	24.8	SY	M
1-Jun-15	Delta Prime Canyon	2711-62709	27.6	SY	F
1-Jun-15	Delta Prime Canyon	2711-62707	32.9	SY	F
1-Jun-15	Delta Prime Canyon	2711-62710	26	ASY	F
4-Jun-15	Technical Area 08	2341-76559	24.4	ASY	M
5-Jun-15	Golf Course	2711-62727	28.4	ASY	F
9-Jun-15	Anchor Ranch	2711-62738	26.6	ASY	M
9-Jun-15	Golf Course	2711-62515	27.4	SY	F
11-Jun-15	Anchor Ranch	2711-62761	24.6	SY	F
11-Jun-15	Anchor Ranch	2711-62760	25.3	SY	F
17-Jun-15	Anchor Ranch	2711-62781	25	ASY	M
17-Jun-15	Anchor Ranch	2711-62780	26.7	SY	M
18-Jun-15	Anchor Ranch	2711-62784	23.1	ASY	M
18-Jun-15	Anchor Ranch	2711-62782	24.1	SY	F
18-Jun-15	Anchor Ranch	2711-62783	24.1	SY	F
18-Jun-15	Anchor Ranch	2711-62785	24.7	ASY	M
19-Jun-15	Anchor Ranch	2711-62798	23.4	SY	M
19-Jun-15	Anchor Ranch	2711-62800	27.3	SY	M
19-Jun-15	Anchor Ranch	2711-62796	23.4	SY	F
19-Jun-15	Anchor Ranch	2711-62799	25.9	ASY	M
19-Jun-15	Anchor Ranch	2711-62801	25.1	ASY	M
26-Jun-15	Ski Hill	2571-92042	24.7	ASY	M
26-Jun-15	Golf Course	2201-98530	24.4	ASY	M
26-Jun-15	Golf Course	2711-62802	24.3	SY	F

After downloading light-level data from the tags, we annotated the twilight times in R packages BAStags (Wotherspoon et al., 2013), TwGeos (Lisovski et al., 2015), and GeoLight (Lisovski andet al., 2012). We identified twilights by setting a threshold light level below which the user has high confidence that the GLS is capturing ambient nighttime light levels. We calibrated our corrected twilight times using both the thresholdCalibration function from SGAT (Sumner et al., 2009) and the Hill-Ekstrom calibration (Hill and Braun, 2001; Lisovski et al., 2012), which has been shown to reduce the error associated with twilight delimitation (Lisovski et al., 2012). We chose calibration periods when birds were most likely to occupy local nestboxes. Threshold-derived locations were fit in SGAT using a Markov chain Monte Carlo simulation of movement trajectories to model probabilities of location (Sumner et al., 2009). We ran SGAT models for 10,000 iterations on three chains after tuning the models from initial runs. We also obtained location estimates from both FlightR (Rakhimberdiev et al., 2017) and Geolight for a subset of two tags using similar calibration techniques.

Methods

We manipulated data and plotted position estimates from the models on maps and visualized the distributions of position estimates in R using the tidyverse (Wickham and Wickham, 2017), ggplot2 (Wickham, 2011), maptools (Lewin-Koh et al., 2012), and raster (Hijmans et al., 2015) packages.

3 RESULTS AND DISCUSSION

Of the 44 tagged individuals, we recaptured 13 at their breeding grounds in 2016, which represented a recapture rate of 29.5%, a value that falls near the higher end of published passerine recapture rates (Arlt et al., 2013; Gómez et al., 2014; Raybuck et al., 2017; Taff et al., 2018). One individual—an apparent window strike—was found dead at Intel Corporation building in Rio Rancho, New Mexico, approximately 78.4 km (straight line distance) from the deployment site near Pajarito Ski Area in Los Alamos County. A second bird was injured by a cat in an unknown location in Albuquerque, New Mexico, in November 2017 and was later brought to a wildlife rescue facility, where the tag was recovered (Table 2-1; red shaded rows). Though the exact recovery location of the bird is unknown, it was recovered a minimum of ~80 km from its deployment site (Table 2-1; red shaded rows). Of the 15 recovered GLSs, we were able to download and analyze data from 10 tags. For brevity, we focus on the location estimation results for GLS unit 30 (which recorded among the clearest light curves) in the main body of the text and compare tag data in Appendix A: and Appendix D:.

An initial analytical step in GLS analyses is the visual inspection of the time series of light levels captured by the GLS. Our data showed clear curves with some noise due to interruption of light levels, likely caused by entering and exiting nestboxes (Figure 3-1 and Figure A-1 through Figure A-10). Light-level noise also varied considerably between individuals and was likely associated with specific light-exposure patterns of individual nestboxes (Figure A-1 through Figure A-10) or habitat types that affected sun exposure. The smooth nature of the curves and lack of deviation from the expected light-level values based on the deployment position suggests that birds remained resident in the area. (Figure 3-1 and Figure A-1 through Figure A-10).

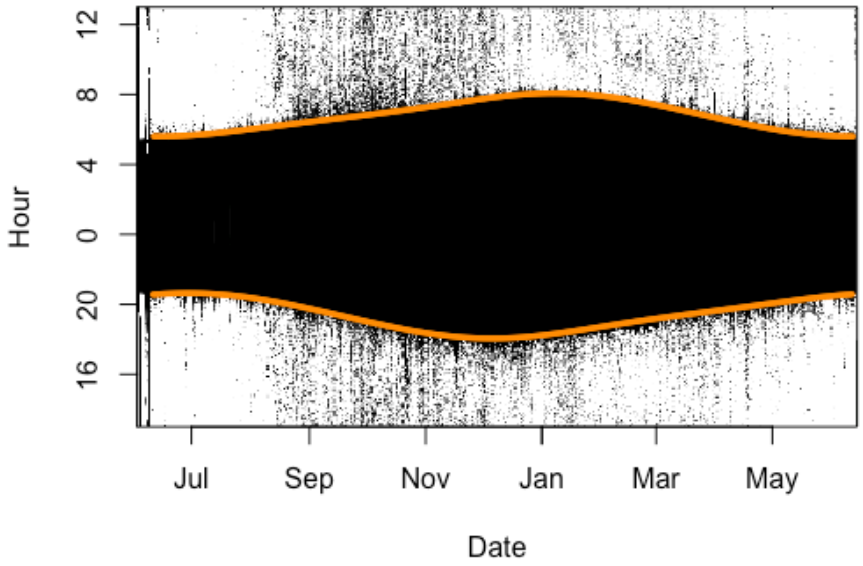

Figure 3-1. Light curve for GLS unit 30 deployed at Anchor Ranch on 9 June 2015 and retrieved at Anchor Ranch Los Alamos County on 13 June 2016. Black region shows low-light conditions from both nestboxes, and night conditions show little deviation with predicted light curve (orange line) based on deployment location. Black streaks illustrate inherent uncertainty in delimiting twilights due to cavity nesting behavior of WEBLs, which contributes to error in methods used to infer geographic locations.

GLS analysis in FlightR, SGAT, and GeoLight all produced highly variable movement tracks with large deviations in latitude, suggesting an inability of the software to extrapolate movement patterns from our light-level data. Small errors in twilight delimitation can lead to large downstream deviations in estimates of latitude (Lisovski et al., 2020). To test for sensitivity to our twilight delimitation, we fit GLS models using both the recommended conservative twilight delimitation approach (Lisovski et al., 2020), where few twilights are manually changed, and a much more liberal approach, where we heavily edited twilight times. Both twilight delimitation strategies produced equivalent results. Additionally, estimation methods can be sensitive to the choice of calibration methods and periods (whether roof-top calibrated or calibrated based on assumed stationary periods). We ran the data for GLS unit 30 under four calibration regimes in SGAT that varied by length of calibration period (10 or 30 assumed stationary days) and method (threshold calibration or Hill-Ekstrom calibration) (Figure B-1). Length of calibration had little impact on location estimates in SGAT, but the Hill-Ekstrom calibration method produced more variable location estimates than the threshold calibration (Figure B-1).

Error introduced through twilight delimitation produced unrealistic latitude estimates for all methods, placing WEBLs well outside their known range, wintering in Nebraska or even northern Canada. Uncertainty in estimates varied substantially between the three estimation methods. GeoLight produced latitude estimates that spanned much of the western hemisphere (Figure C-1). FlightR estimated locations across a longitudinal band spanning the United States (Figure C-1 and Figure C-2). Though consistently

estimating locations well outside realistic locations, often with low probability, SGAT tended to estimate points around the deployment locations (Figure 3-2). None of the methods revealed the expected multi-modal location estimates of migratory species (Cooper et al., 2017; Pedersen et al., 2019; Stutchbury et al., 2009). Most estimates produced either fairly continuous, albeit highly dispersed, clouds of location estimates as with SGAT or longitudinal bands with multiple stationary sites well beyond the species' known range (FlightR and GeoLight) (Figure C-1, Figure C-2, and Figure D-1 through Figure D-17). FlightR showed extreme sensitivity to prior specification of the maximum distance a bird is allowed to move between twilights, and changes in these values changed the latitudinal extent of estimated tracks by >10 degrees (Figure C-2). Our longitudinal estimates remained centered around the deployment longitude for most GLSs, whereas latitude was most subject to estimation error likely due to the cavity nesting behavior of the species. Although some units generated bimodal location estimates (Figure D-3, Figure D-5, and Figure D-9), the estimates were not biologically plausible given what we know of the specie's range or expect from known migratory behaviors. The low resolution of GLS analyses could lead to over-interpretation (Lisovski et al., 2018). Because GLS analysis is ineffective if animals travel under 200 km, which represents the margin of error for all geolocation analyses (Lisovski et al., 2020), the most parsimonious explanation for our results is that WEBLs in this area are resident or do not migrate sufficient distances to be captured by GLSs.

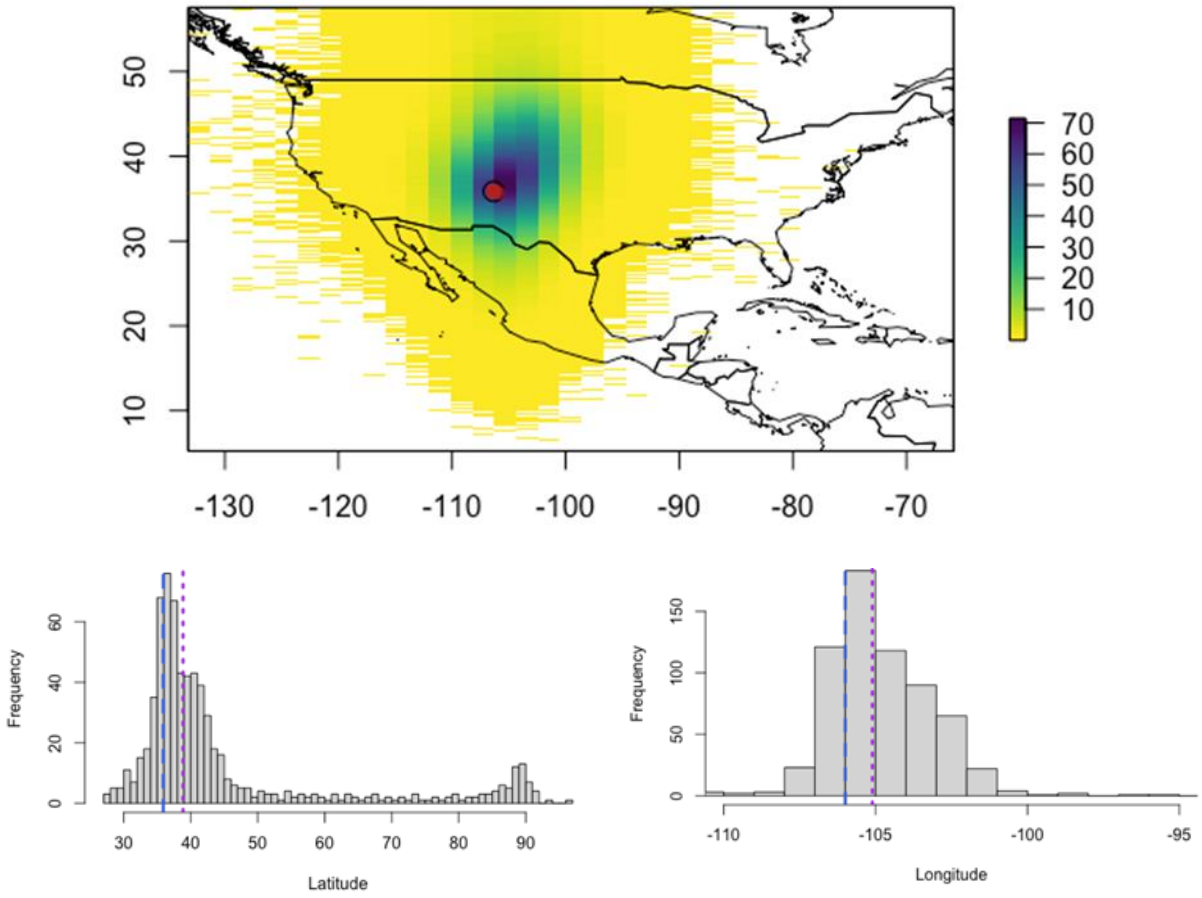

Figure 3-2. Probability heat map generated in R package SGAT of location estimates for GLS unit 30 deployed from the Anchor Ranch nestbox sites on 9 June 2015. Darker colors indicate higher probability of the GLS position. Note single cluster of high probabilities, indicating either resident behavior or migratory behavior below the margin of error for light-level geolocation analysis. Bottom two panels show mean latitude distribution (left) and mean longitude distribution (right). Blue dashed lines indicate coordinates of deployment, whereas purple dashed lines indicate median of mean latitude and longitude estimates.

The SGAT position estimates, in context with the shape of the light curves, and the two individuals recovered in late fall from <100 km (straight-line distance) southeast of the deployment locations suggest that the LANL population of WEBLs does not undertake long-distance migrations. However, the recovery of two individuals ~80 km southeast and ~600 m lower in elevation than LANL breeding sites suggests at least some members of the LANL population undertake short-distance, elevational migrations seasonally. The position of the LANL WEBL breeding population at the edge of putatively migrant populations to the north and the steady trend in WEBL observations throughout the county drive the possibility of seasonal replacement of breeding birds at LANL. In this hypothetical scenario, a portion or all of the LANL breeding population of WEBLs undertakes short-distance (<200 km) migrations,

wintering at lower elevations and latitudes—whereas more northern populations from northern New Mexico and the Colorado Rocky Mountains overwinter in Los Alamos County. To test the validity of this scenario and understand migratory bird movements at higher resolution around LANL, biologists would need to tag birds with satellite transmitter or pinpoint GPS tags (Johnson et al., 2020; Marquardt et al., 2012; Rowley, 2017). These tags can uncover shorter distance migrations across elevation, temperature, and other environmental gradients that may be more commonplace than previously thought. In the meantime, LANL biologists will adapt this report to a scientific journal format for submission to peer-reviewed journals to contribute to a paucity of literature on short-distance and elevational migration patterns.

Although delimiting unrecognized migratory behaviors in local WEBLs will not impact LANL project compliance or the management strategies of the ANN, this knowledge could influence our understanding of the impacts of legacy waste and operational chemical use on wildlife as well as contribute to our regional understanding of migratory birds as good site stewards. The ANN has been a source of biological samples for the analysis of legacy waste and chemical constituents since its inception in 1997. Both the Soils Foodstuffs and Biota Program and the Bioscience Division have tested nonviable WEBL eggs and tissues for constituents of interest (Fair and Myers, 2002; Gaukler et al., 2018a; Gaukler et al., 2018b). An important assumption behind this data-gathering process is that WEBLs remain resident at LANL throughout the year. If birds are not resident, tissues recovered from different seasons may not reflect local chemical conditions at LANL. Beyond this important logistical concern, LANL can only strengthen their position as a local steward of the environment by uncovering ecological and natural history phenomena relevant to the Pajarito Plateau and northern New Mexico more generally.

4 REFERENCES

Abeyta, E. J., Bartlow, A. W., Hathcock, C. D., and Fair, J. M. (2021). Individual Nest Site Preferences Do Not Explain Upslope Population Shifts of a Secondary Cavity-Nesting Species. *Animals, 11*(8), 2457. Retrieved from https://www.mdpi.com/2076-2615/11/8/2457

All About Birds (AAB). (2019a). Western Bluebird. Retrieved from https://www.allaboutbirds.org/guide/Western_Bluebird

All About Birds (AAB). (2019b). Western Bluebird. Retrieved from https://www.allaboutbirds.org/guide/Western_Bluebird/maps-range

Arlt, Debora, Matthew Low, and Tomas Pärt. (2013). Effect of Geolocators on Migration and Subsequent Breeding Performance of a Long-Distance Passerine Migrant. *PLOS ONE* 8 (12): e82316. https://doi.org/10.1371/journal.pone.0082316

Cooper, N. W., Hallworth, M. T., and Marra, P. P. (2017). Light-level geolocation reveals wintering distribution, migration routes, and primary stopover locations of an endangered long-distance migratory songbird. *Journal of Avian Biology, 48*(2), 209–219. https://doi.org/10.1111/jav.01096

Delmore, K. E., Fox, J. W., and Irwin, D. E. (2012). Dramatic intraspecific differences in migratory routes, stopover sites and wintering areas, revealed using light-level geolocators. *Proceedings of the Royal Society B: Biological Sciences, 279*(1747), 4582–4589. https://doi.org/10.1098/rspb.2012.1229

eBird. (2021). Western Bluebird. *eBird: An online database of bird distribution and abundance [web application]*.

Fair, J. M., and Myers, O. B. (2002). Early reproductive success of western bluebirds and ash-throated flycatchers: a landscape-contaminant perspective. *Environmental Pollution, 118*(3), 321–330. https://doi.org/10.1016/S0269-7491(01)00302-5

Gaukler, S. M., Hathcock, C. D., and Fair, J. M. (2018a). Inorganic Elements in Eggs of Two Cavity-Nesting Passerine Species at and around Los Alamos National Laboratory, Los Alamos, New Mexico. *Journal of Environmental Protection, 9* (LA-UR-16-24852).

Gaukler, S. M., Hathcock, C. D., and Fair, J. M. (2018b). Organic chemical concentrations in eggs and nestlings of cavity nesting birds at and around Los Alamos National Laboratory. *Journal of Environmental and Analytical Toxicology, 8* (LA-UR-16-25345).

Gómez, Jesús, Chantel I. Michelson, David W. Bradley, D. Ryan Norris, Lisha L. Berzins, Russell D. Dawson, and Robert G. Clark. (2014). Effects of geolocators on reproductive performance and annual return rates of a migratory songbird. *Journal of Ornithology* 155 (1): 37–44. https://doi.org/10.1007/s10336-013-0984-x

Guinan, J. A., Gowaty, P. A., and Eltzroth, E. K. (2008). Western Bluebird (Sialia mexicana). *The Birds of North America.* Version 2.0. Retrieved from https://doi.org/10.2173/bna.510

Hijmans, R. J., Van Etten, J., Cheng, J., Mattiuzzi, M., Sumner, M., Greenberg, J. A., Lamigueiro, O. P., Bevan, A., Racine, E. B., Shortridge, A. and Hijmans, M. R. J., (2015). Package 'raster'. R package, 734.

References

Hill, R. D., and Braun, M. J. (2001). Geolocation by Light Level. In J. R. Sibert and J. L. Nielsen (Eds.), *Electronic Tagging and Tracking in Marine Fisheries: Proceedings of the Symposium on Tagging and Tracking Marine Fish with Electronic Devices, February 7–11, 2000, East-West Center, University of Hawaii* (pp. 315–330). Dordrecht: Springer Netherlands.

Johnson, O. W., Tibbitts, T. L., Weber, M. F., Bybee, D. R., Goodwill, R. H., Bruner, A. E., . . . Brooks, D. C. (2020). Tracking the migration of Pacific Golden-Plovers from nonbreeding grounds at Moorea, French Polynesia, using Pinpoint GPS-Argos tags. *Wader Study, 127*(1), 53–59.

Lewin-Koh, N. J., Bivand, R., Pebesma, J., Archer, E., Baddeley, A., Giraudoux, D. G., Rubio, V. G. m., Hausmann, P., Hufthammer, K. O., and Jagger, T. (2012). Package 'maptools'. Internet: http://cran.r-project.org/web/packages/maptools/maptools.pdf (30.1. 2012).

Lisovski, S., Bauer, S., Briedis, M., Davidson, S. C., Dhanjal-Adams, K. L., Hallworth, M. T., Karagicheva, J., Meier, C. M., Merkel, B., Ouwehand, J., Pedersen, L., Rakhimberdiev, E., Roberto-Charron, A., Seavy, N. E., Sumner, M. D., Taylor, C. M., Wotherspoon, S. J., and Bridge, E. S. (2020). Light-level geolocator analyses: A user's guide. *Journal of Animal Ecology* 89(1): 221–236. https://doi.org/10.1111/1365-2656.13036.

Lisovski, S., Hewson, C. M., Klaassen, R. H. G., Korner-Nievergelt, F., Kristensen, M. W., and Hahn, S. (2012). Geolocation by light: accuracy and precision affected by environmental factors. *Methods in Ecology and Evolution, 3*(3), 603–612. https://doi.org/10.1111/j.2041-210X.2012.00185.x

Lisovski, S., Schmaljohann, H., Bridge, E. S., Bauer, S., Farnsworth, A., Gauthreaux, S. A., Jr., Hahn, S., Hallworth, M. T., Hewson, C. M., Kelly, J. F., Liechti, F., Marra, P. P., Rakhimberdiev, E., Ross, J. D., Seavy, N. E., Sumner, M. D., Taylor, C. M., Winkler, D. W., Wotherspoon, S. J., and Wunder, M. B. (2018). Inherent limits of light-level geolocation may lead to over-interpretation. *Current Biology* 28(3): R99–R100. https://doi.org/10.1016/j.cub.2017.11.072

Lisovski, S., Sumner, M. D., and Wotherspoon, S. J. (2015). TwGeos: Basic data processing for light based geolocation archival tags. Github Repository: Github Repository. Retrieved from https://github.com/slisovski/TwGeos

Marquardt, D. D., Scroggs, L., Pierce, B. L., Skow, K. L., Mote, K. D., and Collier, B. A. (2012). Assessment of GPS Transmitters for Use on Northern Bobwhite Quail. *Journal of the Southeastern Association of Fish and Wildlife Agencies, 4*, 100–108.

Møller, A. P., Garamszegi, L. Z., Peralta-Sánchez, J. M., and Soler, J. J. (2011). Migratory divides and their consequences for dispersal, population size and parasite–host interactions. *Journal of Evolutionary Biology, 24*(8), 1744–1755. https://doi.org/10.1111/j.1420-9101.2011.02302.x

Pedersen, L., Thorup, K., and Tøttrup, A. P. (2019). Annual GPS tracking reveals unexpected wintering area in a long-distance migratory songbird. *Journal of Ornithology, 160*(1), 265–270. doi:10.1007/s10336-018-1610-8

Rakhimberdiev, E., Saveliev, A., Piersma, T., and Karagicheva, J. (2017). FLightR: an R package for reconstructing animal paths from solar geolocation loggers. *Methods in Ecology and Evolution, 8*(11), 1482–1487. https://doi.org/10.1111/2041-210X.12765

Rappole, J. H., and Tipton, A. R. (1991). New Harness Design for Attachment of Radio Transmitters to Small Passerines (Nuevo Diseño de Arnés para Atar Transmisores a Passeriformes Pequeños). *Journal of Field Ornithology, 62*(3), 335–337. Retrieved from http://www.jstor.org/stable/20065798

Raybuck, Douglas W., Jeffrey L. Larkin, Scott H. Stoleson, and Than J. Boves. (2017). Mixed effects of geolocators on reproduction and survival of Cerulean Warblers, a canopy-dwelling, long-distance migrant. *The Condor: Ornithological Applications* 119 (2): 289–297.

References

Rowley, R. J. (2017). Pinpoint: How GPS is Changing Technology, Culture, and Our Minds. *The AAG Review of Books, 5*(3), 195–196. https://doi:10.1080/2325548X.2017.1315256

Rutz, C., and Hays, G. C. (2009). New frontiers in biologging science. *Biology Letters, 5*(3), 289–292. https://doi:10.1098/rsbl.2009.0089

Streby, H. M., McAllister, T. L., Peterson, S. M., Kramer, G. R., Lehman, J. A., and Andersen, D. E. (2015). Minimizing marker mass and handling time when attaching radio-transmitters and geolocators to small songbirds. *The Condor, 117*(2), 249-255. https://doi:10.1650/CONDOR-14-182.1

Stutchbury, B. J., Tarof, S. A., Done, T., Gow, E., Kramer, P. M., Tautin, J., Fox, J. W., and Afanasyev, V. (2009). Tracking long-distance songbird migration by using geolocators. *Science* 323(5916): 896–896.

Sumner, M. D., Wotherspoon, S. J., and Hindell, M. A. (2009). Bayesian Estimation of Animal Movement from Archival and Satellite Tags. *PLOS ONE, 4*(10), e7324–e7324. https://doi:10.1371/journal.pone.0007324

Taff, C. C., C. R. Freeman-Gallant, H. M. Streby, and G. R. Kramer. (2018). Geolocator deployment reduces return rate, alters selection, and impacts demography in a small songbird. *PLOS ONE*, 13(12): e0207783. https://doi.org/10.1371/journal.pone.0207783

Wickham, H. (2011). ggplot2. *Wiley Interdisciplinary Reviews: Computational Statistics, 3*(2), 180–185.

Wickham, H., and Wickham, M. H. (2017). Package tidyverse. *Easily Install and Load the 'Tidyverse'*.

Wikelski, M., Kays, R. W., Kasdin, N. J., Thorup, K., Smith, J. A., and Swenson, G. W., Jr. (2007). Going wild: what a global small-animal tracking system could do for experimental biologists. *Journal of Experimental Biology, 210*(2), 181–186. https://doi:10.1242/jeb.02629

Wotherspoon, S. J., Sumner, M. D., and Lisovski, S. (2013). R Package BAStag: Basic data processing for light based geolocation archival tags. Retrieved from https://github.com/SWotherspoon/SGAT

Wysner, T. E., Bartlow, A. W., Hathcock, C. D., and Fair, J. M. (2019). Long-term phenology of two North American secondary cavity-nesters in response to changing climate conditions. *The Science of Nature, 106*(9), 54. https://doi:10.1007/s00114-019-1650-9

5 ACKNOWLEDGMENTS

We thank Brent Thompson for helping to develop the GLS harness procedures and the tag deployments and retrievals. We thank the following personnel for field and logistical support: Emily Phillips and Maria Musgrave. Special thanks to Dr. Henry Streby (University of Toledo) for mentoring in harness development and deployment procedures. This work was conducted under an approved IACUC protocol and both federal and state permits.

6 ACRONYMS

Acronym	Definition
ANN	Avian Nestbox Network
CDB	Cañada del Buey
CI	Confidence Interval
GC	Golf Course
GLS	global/geographic location sensor
GMT	Greenwich Mean Time
IACUC	Institutional Animal Care & Use Committee
LANL	Los Alamos National Laboratory
WEBL	Western Bluebird

Appendix A: GLS Light Curves

Light-level noise is generated by birds entering and exiting nestboxes throughout the day. Light curves are presented for the eight GLS with downloadable data. Notice that all light curves follow the predicted light curve for the deployment location (orange lines), indicating little movement from breeding grounds. Variability in light-level noise is shown as black streaks in the light curve. Additional light-level noise is likely due to the specific light-exposure environment of each nestbox.

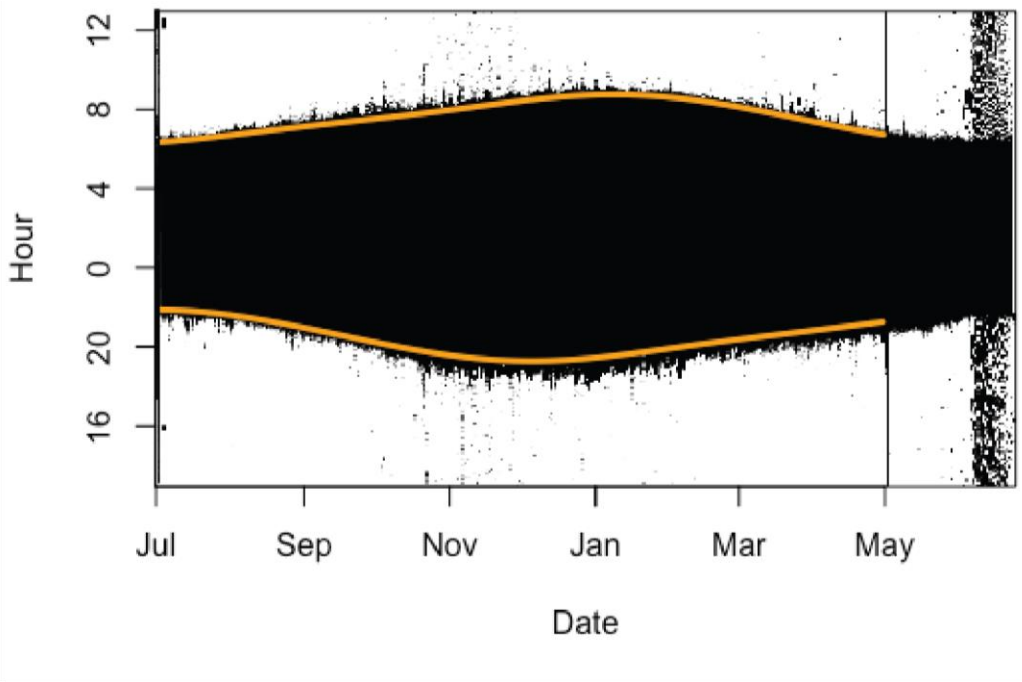

Figure A-1. Light curve for GLS unit 3 in GMT deployed at Cañada del Buey (CDB) on 26 June 2015 and retrieved at Ski Hill, Los Alamos County, on 23 June 2016. Black region shows low-light conditions from both nestboxes, and night conditions show little deviation with predicted light curve (orange line).

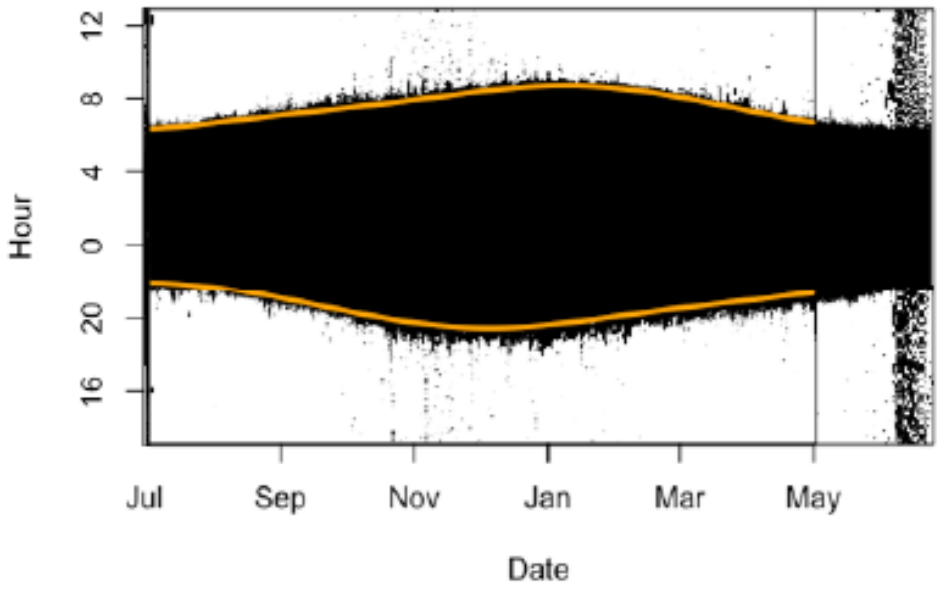

Figure A-2. Light curve for GLS unit 18 deployed at CDB on 1 June 2015 and retrieved at CDB, Los Alamos County, on 17 June 2016. Black region shows low-light conditions from both nestboxes, and night conditions show little deviation with predicted light curve (orange line).

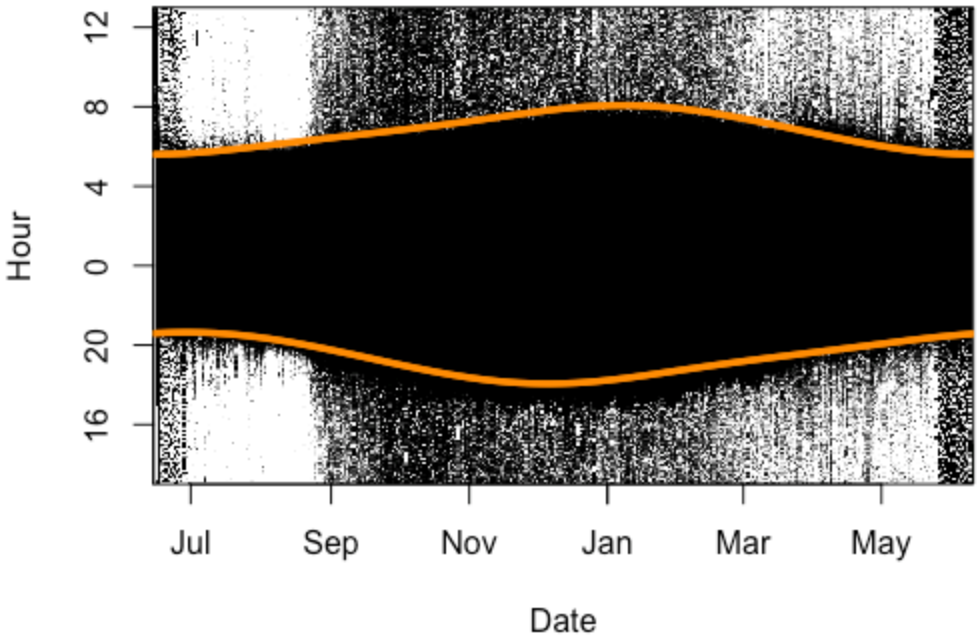

Figure A-3. Light curve for GLS unit 19 deployed at Anchor Ranch on 17 June 2015 and retrieved at Anchor Ranch, Los Alamos County, on 9 June 2016. Black region shows low-light conditions from both nestboxes, and night conditions show little deviation with predicted light curve (orange line).

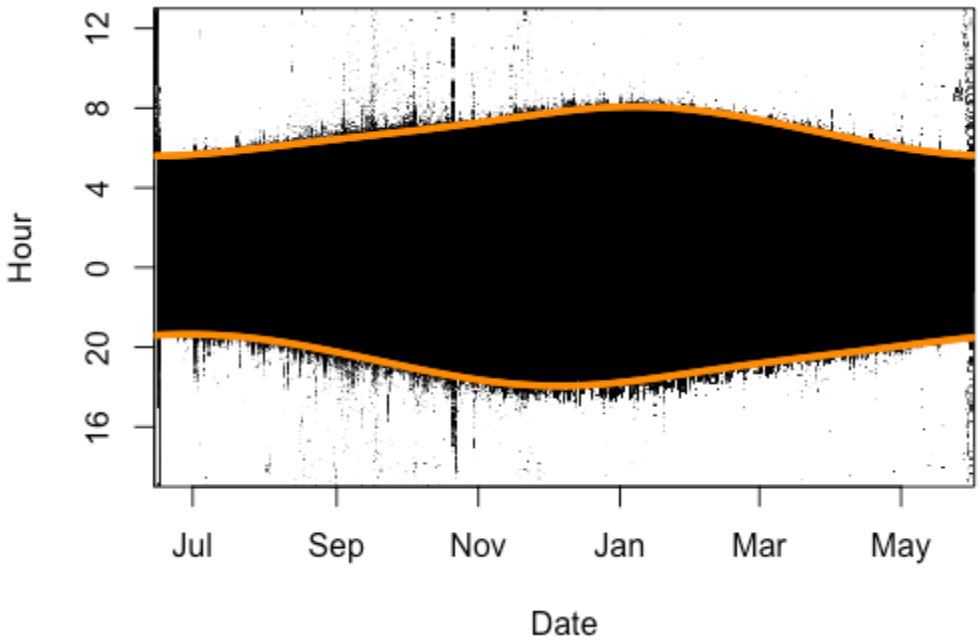

Figure A-4. Light curve for GLS unit 21 deployed at Anchor Ranch on 17 June 2015 and retrieved at Anchor Ranch, Los Alamos County, on 31 May 2016. Black region shows low-light conditions from both nestboxes, and night conditions show little deviation with predicted light curve (orange line).

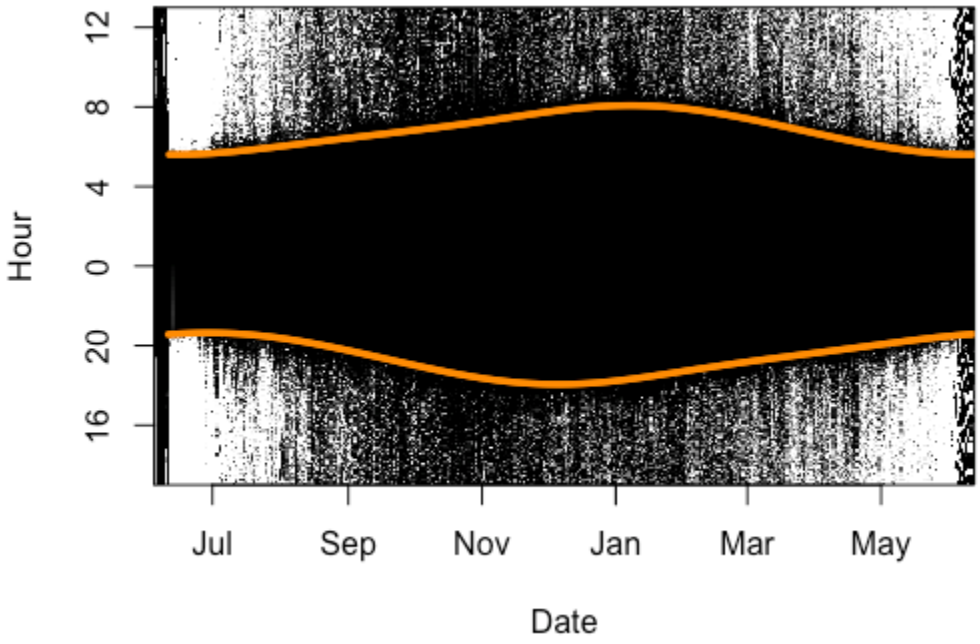

Figure A-5. Light curve for GLS unit 23 deployed at Anchor Ranch on 11 June 2015 and retrieved at Anchor Ranch, Los Alamos County, on 12 June 2016. Black region shows low-light conditions from both nestboxes, and night conditions show little deviation with predicted light curve (orange line).

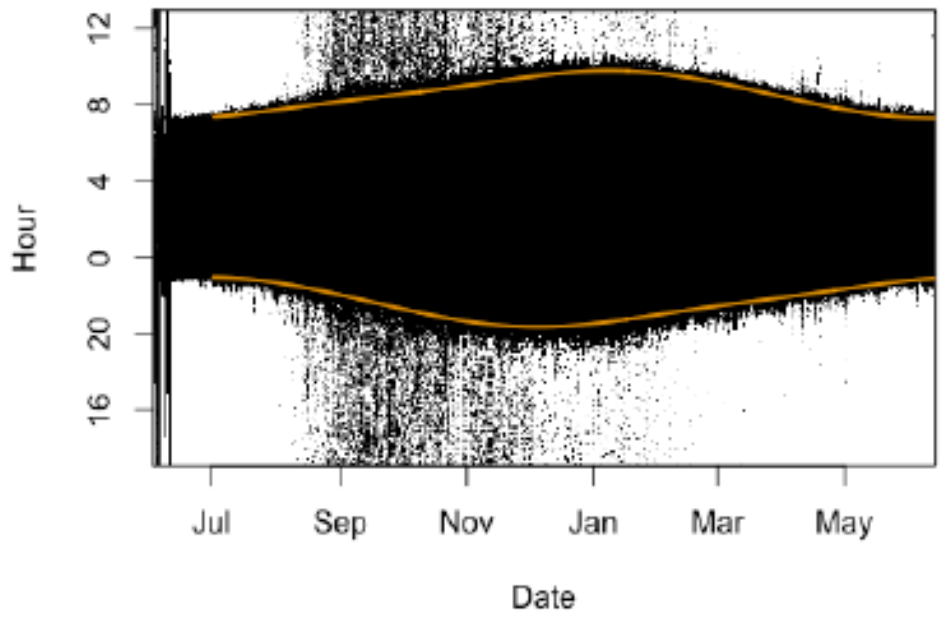

Figure A-6. Light curve for GLS unit 25 in GMT deployed at Anchor Ranch on 11 June 2015 and retrieved at Anchor Ranch, Los Alamos County, on 12 June 2016. Black region shows low-light conditions from both nestboxes, and night conditions show little deviation with predicted light curve (orange line).

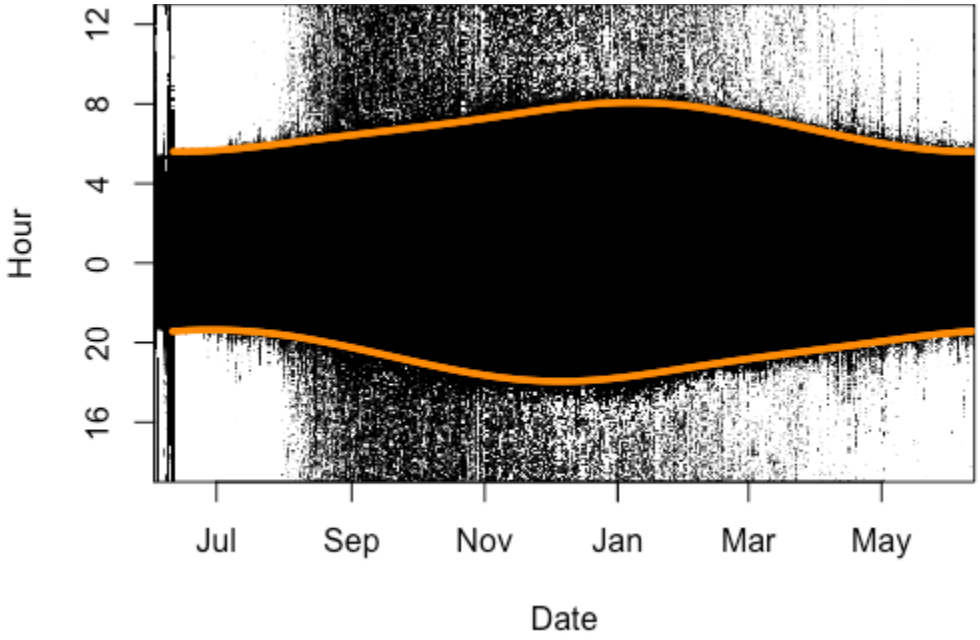

Figure A-7. Light curve for GLS unit 27 deployed at Golf Course (GC) on 5 June 2015 and retrieved at GC, Los Alamos County, on 16 June 2016. Black region shows low-light conditions from both nestboxes, and night conditions show little deviation with predicted light curve (orange line).

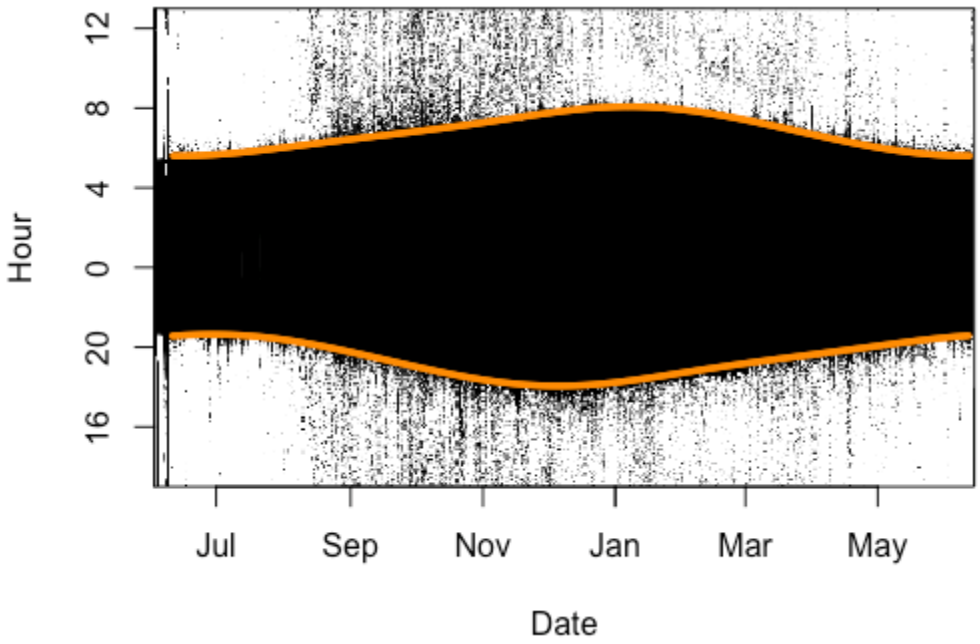

Figure A-8. Light curve for GLS unit 30 deployed at Anchor Ranch on 9 June 2015 and retrieved at Anchor Ranch, Los Alamos County, on 13 June 2016. Black region shows low-light conditions from both nestboxes, and night conditions show little deviation with predicted light curve (orange line).

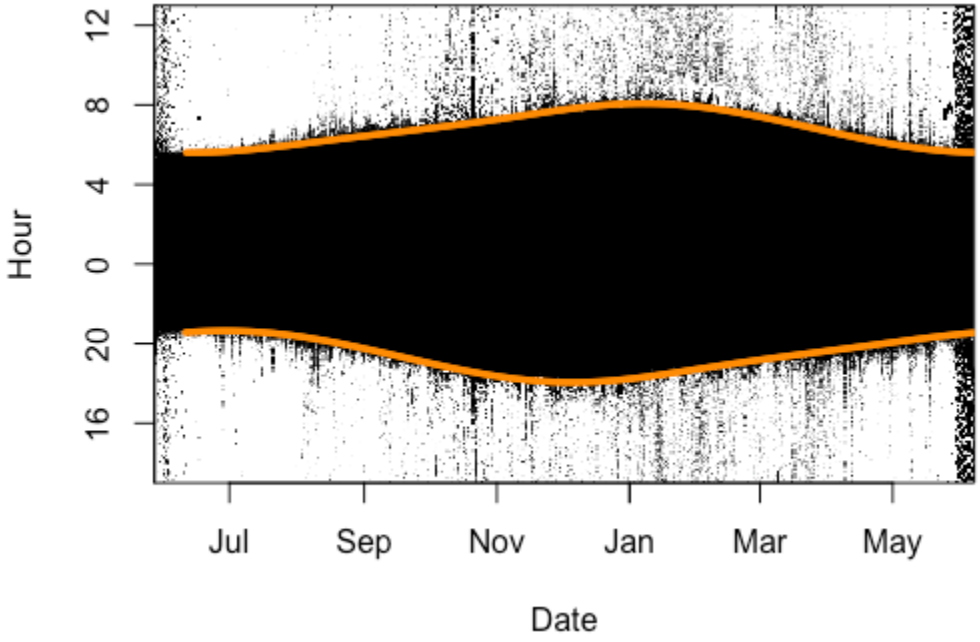

Figure A-9. Light curve for GLS unit 38 deployed at Sandia on 28 May 2015 and retrieved at Sandia, Los Alamos County, on 6 June 2016. Black region shows low-light conditions from both nestboxes, and night conditions show little deviation with predicted light curve (orange line).

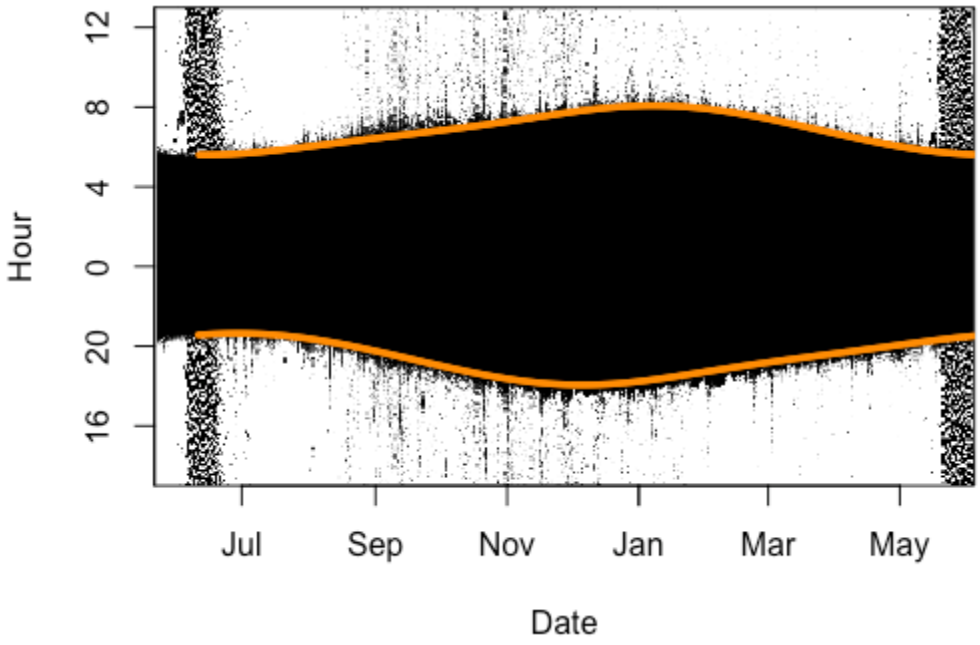

Figure A-10. Light curve for GLS unit 42 deployed at GC on 22 May 2015 and retrieved at GC, Los Alamos County, on 3 June 2016. Black region shows low-light conditions from both nestboxes, and night conditions show little deviation with predicted light curve (orange line).

Appendix B: SGAT Calibration Comparison

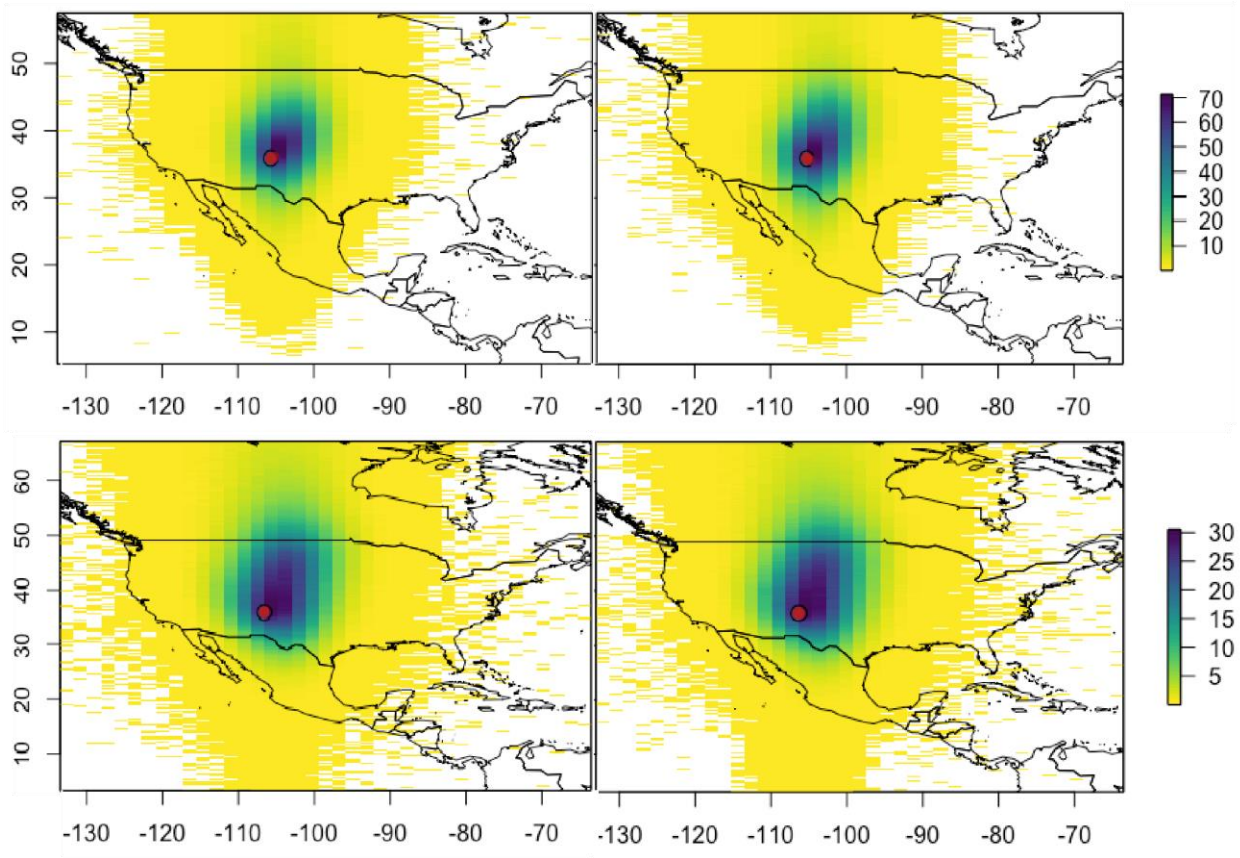

Figure B-1. Comparison of calibration methods for SGAT location estimation of GLS unit 30. Left panels are 10-day calibration period, and right panels are 30-day calibration period. Top panels show threshold calibration method, and bottom panels show Hill-Ekstrom calibration. Note that location estimates from Hill-Ekstrom method have lower probability and larger uncertainty than estimates from threshold calibration method.

Appendix C: Comparison of Location Estimation Methods

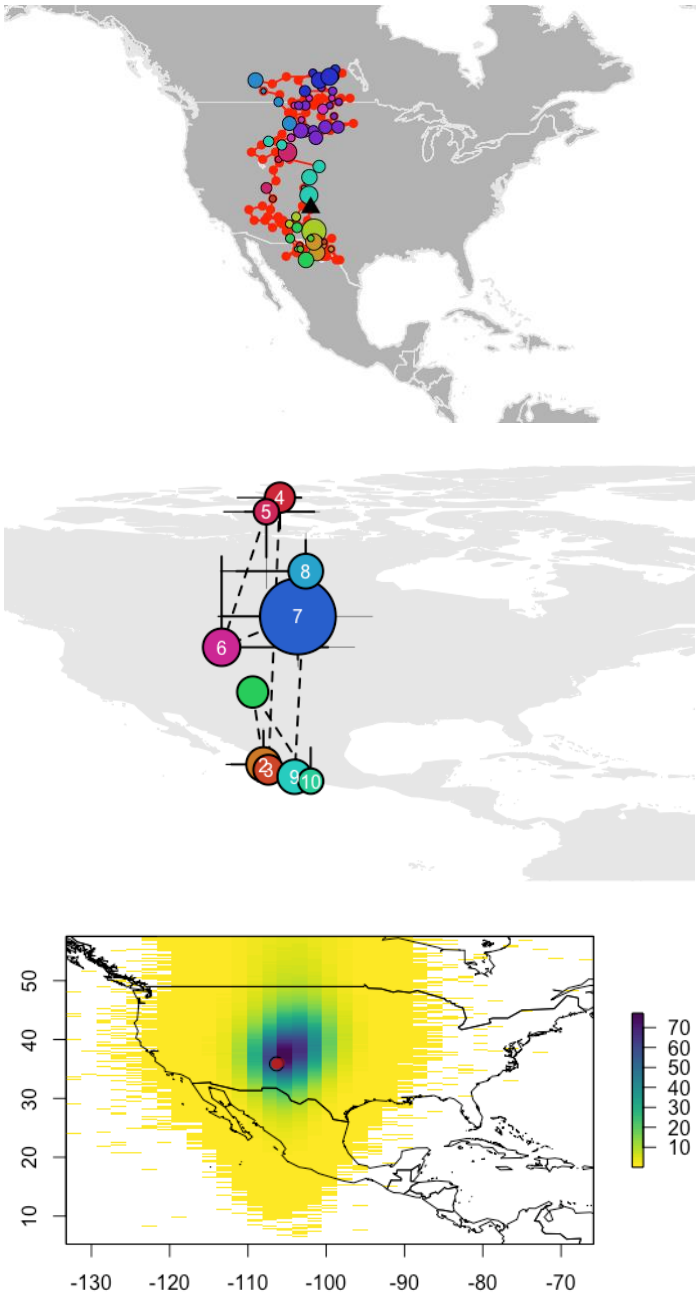

Figure C-1. Three estimation methods from GLS unit 30 using same 30-day calibration period. Top panel shows estimation produced in FlightR (black triangle indicates deployment location). Middle panel shows estimations produced by GeoLight (green circle indicates deployment location). Bottom panel shows estimations produced by SGAT (red circle indicates deployment location). Colors in top and middle panels represent months in which stationary periods were estimated and are not described because estimation error rendered them meaningless.

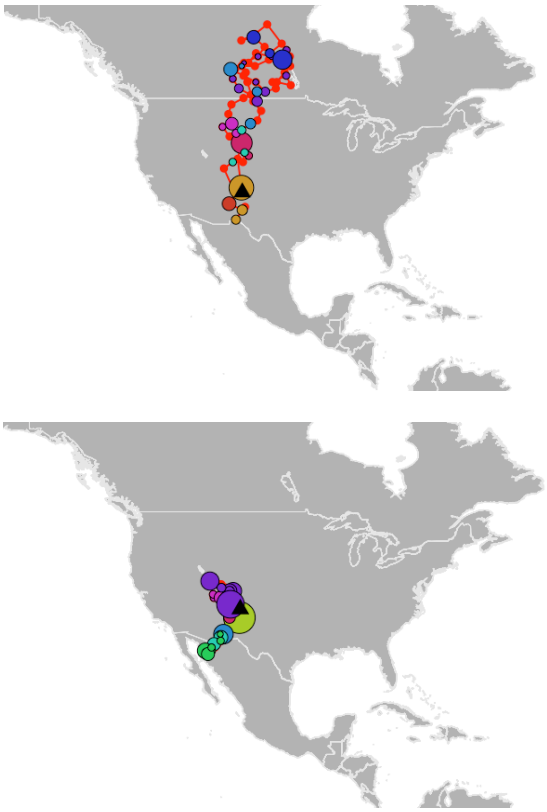

Figure C-2. Two FlightR tracks estimated from GLS unit 25 using the same 30-day calibration period but varying the model parameter that describes the distance allowed to move between twilights from 1000 km (top) to 100 km (bottom). Black triangles show deployment locations. Note extreme sensitivity to prior specification in model. Colors represent month of stopover and are irrelevant here.

Appendix D: FULL SGAT RESULTS

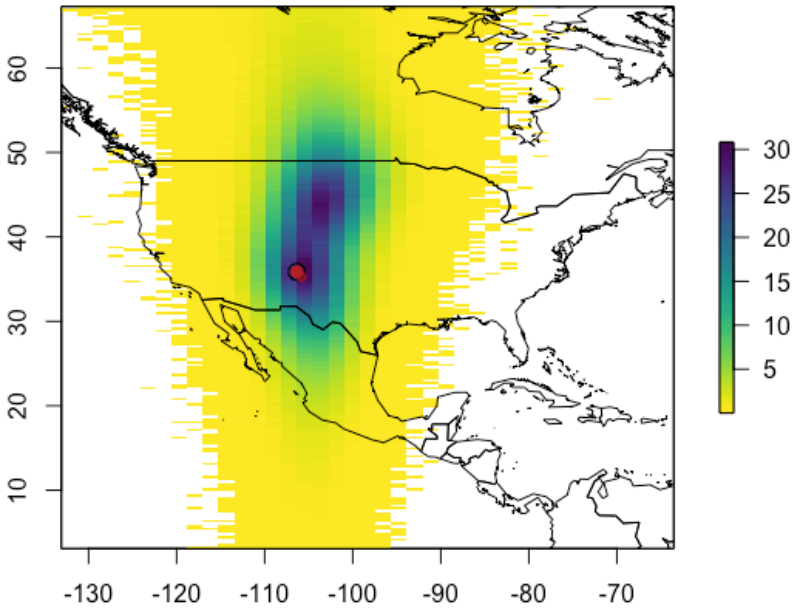

Figure D-1. SGAT-generated probability of location map for GLS unit 3, truncated to show area of highest probability estimates (see scale on left). Red circle shows deployment location.

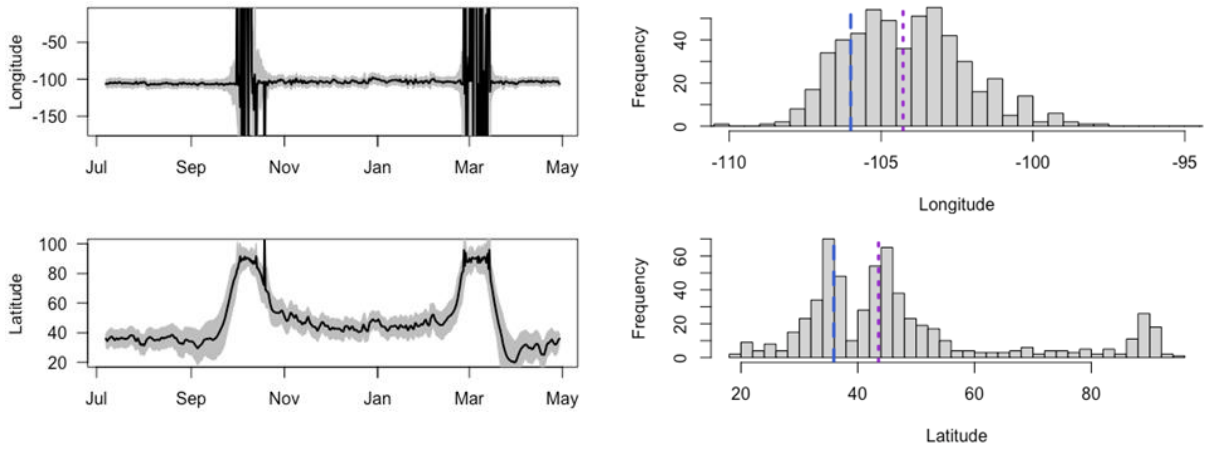

Figure D-2. Latitude and longitude estimates from SGAT analyses of GLS unit 3, truncated to show highest probability estimates. Left panel shows estimated latitude and longitude through time with gray 95% CI interval. Note extreme variation is expected around equinoxes. Right panel shows mean estimates from 10,000 iterations of SGAT model for longitude and latitude. Blue dashed lines show deployment locations; purple dashed lines show median of mean estimates.

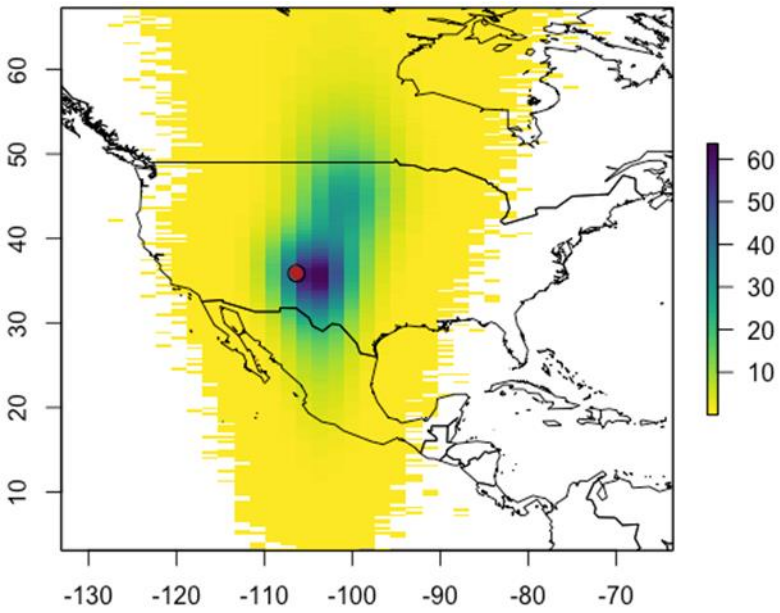

Figure D-3. SGAT-generated probability of location map for GLS unit 18, truncated to show area of highest probability estimates (see scale on left). Red circle shows deployment location.

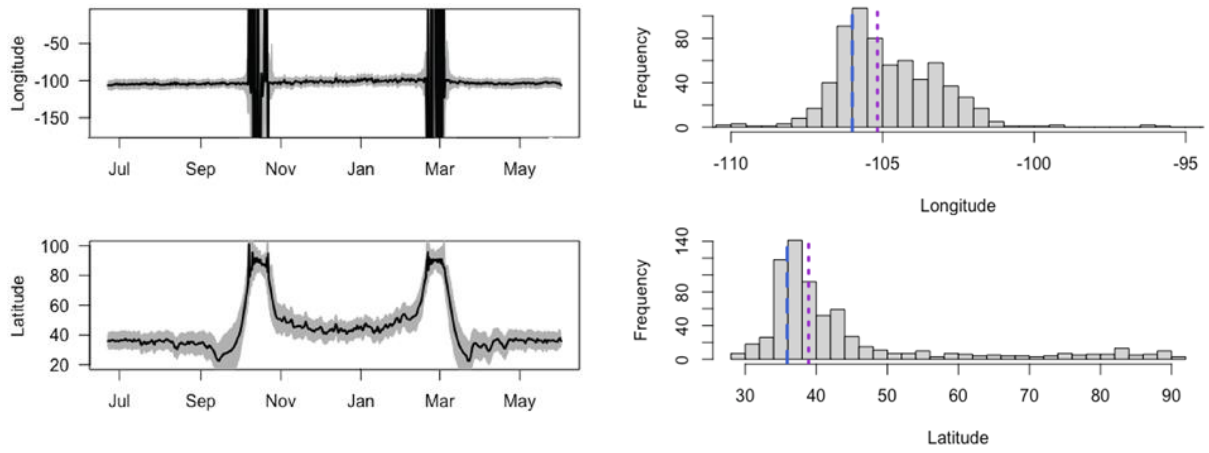

Figure D-4. Latitude and longitude estimates from SGAT analyses of GLS unit 18, truncated to show highest probability estimates. Left panel shows estimated latitude and longitude through time with gray 95% CI interval. Note extreme variation is expected around equinoxes. Right panel shows mean estimates from 10,000 iterations of SGAT model for longitude and latitude. Blue dashed lines show deployment locations; purple dashed lines show median of mean estimates.

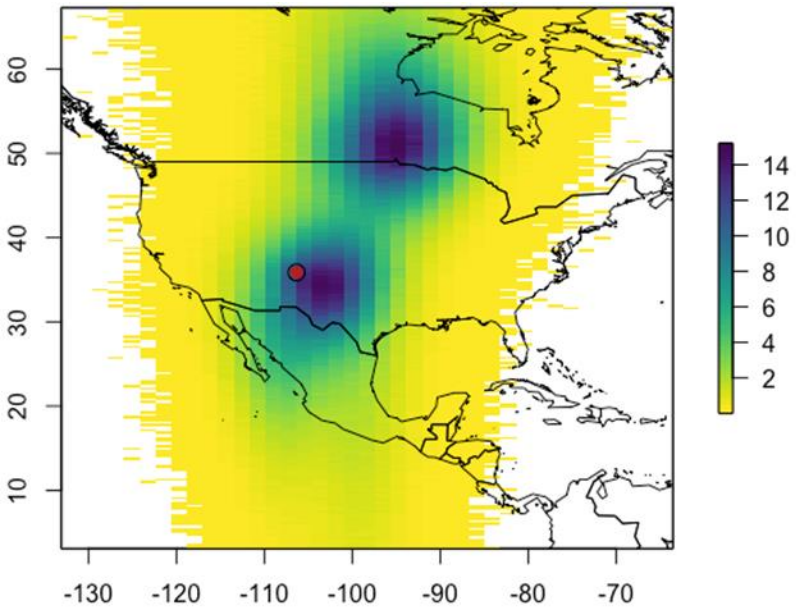

Figure D-5. SGAT-generated probability of location map for GLS unit 19, truncated to show area of highest probability estimates (see scale on left). Red circle shows deployment location.

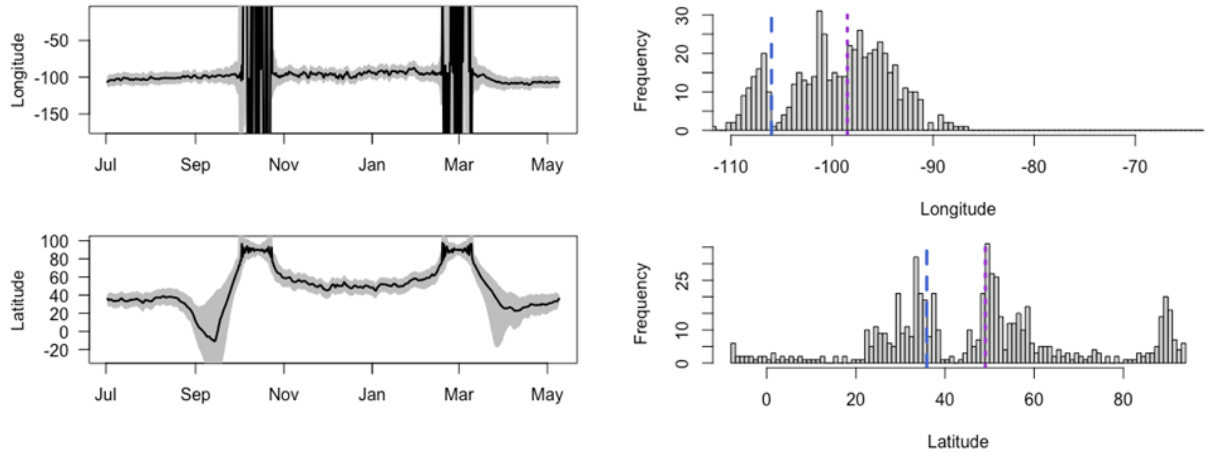

Figure D-6. Latitude and longitude estimates from SGAT analyses of GLS unit 19, truncated to show highest probability estimates. Left panel shows estimated latitude and longitude through time with gray 95% CI interval. Note extreme variation is expected around equinoxes. Right panel shows mean estimates from 10,000 iterations of SGAT model for longitude and latitude. Blue dashed lines show deployment locations; purple dashed lines show median of mean estimates.

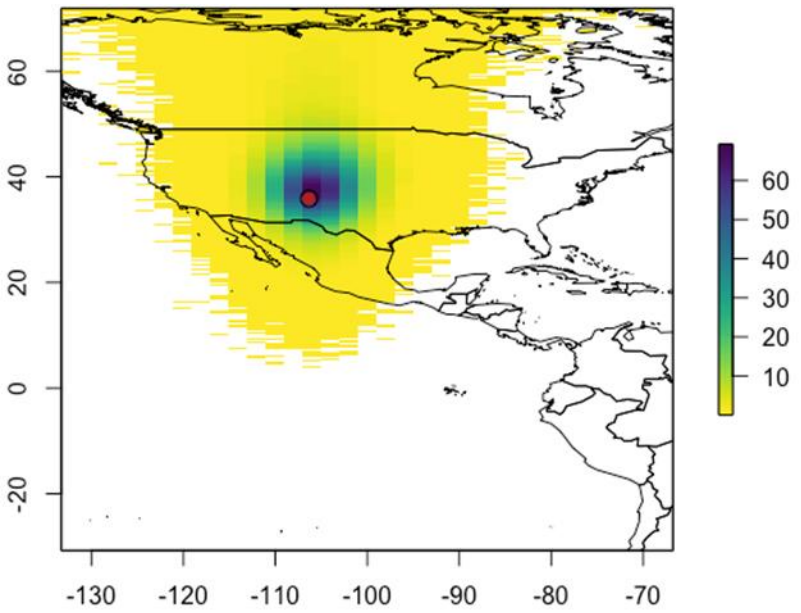

Figure D-7. SGAT-generated probability of location map for GLS unit 21, truncated to show area of highest probability estimates (see scale on left). Red circle shows deployment location.

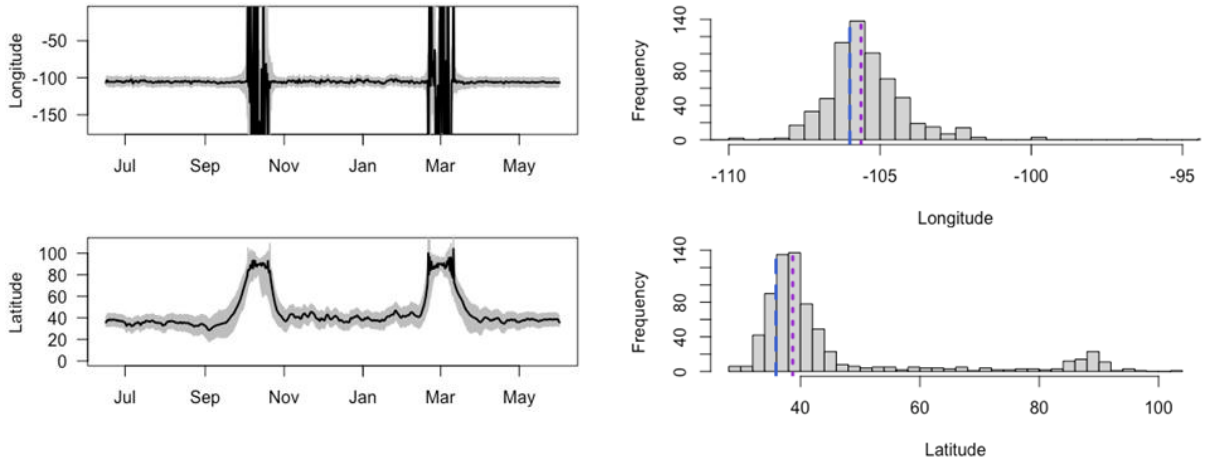

Figure D-8. Latitude and longitude estimates from SGAT analyses of GLS unit 21, truncated to show highest probability estimates. Left panel shows estimated latitude and longitude through time with gray 95% CI interval. Note extreme variation is expected around equinoxes. Right panel shows mean estimates from 10,000 iterations of SGAT model for longitude and latitude. Blue dashed lines show deployment locations; purple dashed lines show median of mean estimates.

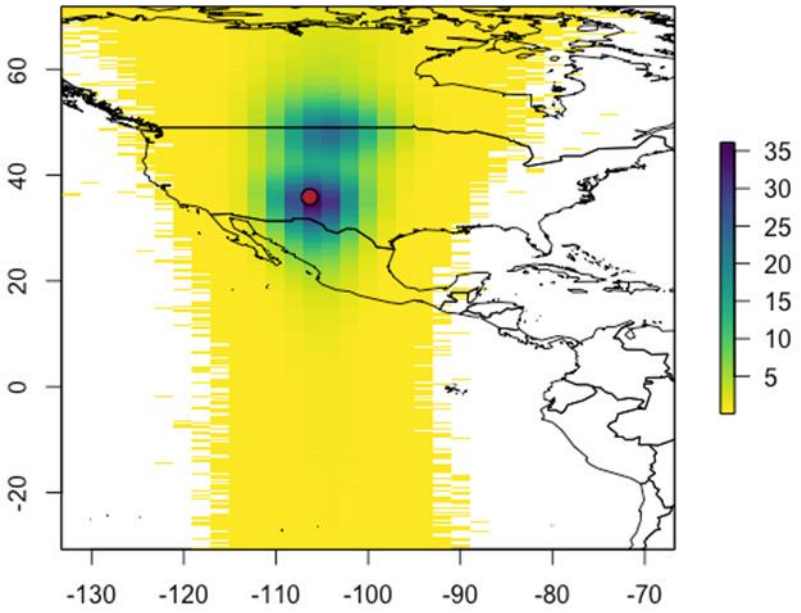

Figure D-9. SGAT-generated probability of location map for GLS unit 25, truncated to show area of highest probability estimates (see scale on left). Red circle shows deployment location.

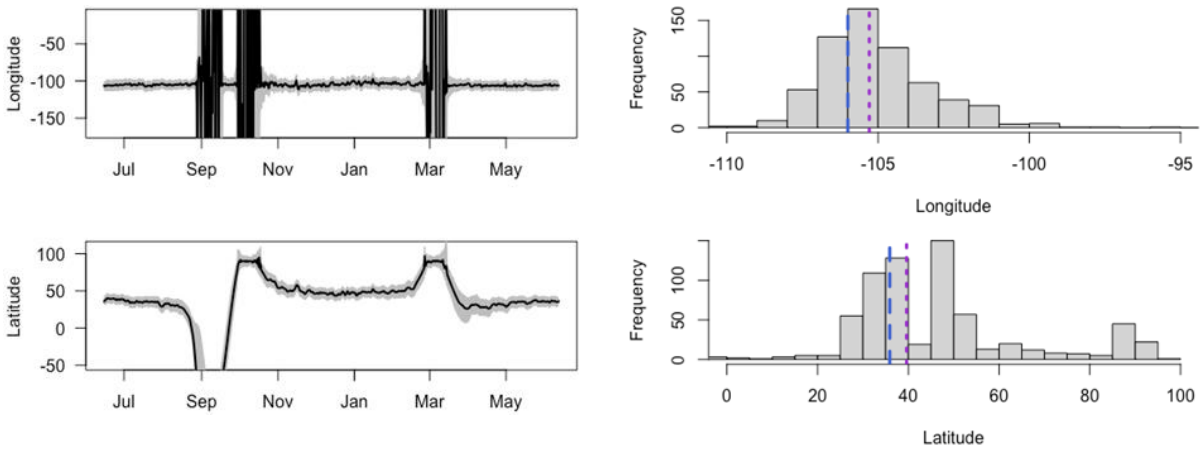

Figure D-10. Latitude and longitude estimates from SGAT analyses of GLS unit 25, truncated to show highest probability estimates. Left panel shows estimated latitude and longitude through time with gray 95% CI interval. Note extreme variation is expected around equinoxes. Right panel shows mean estimates from 10,000 iterations of SGAT model for longitude and latitude. Blue dashed lines show deployment locations; purple dashed lines show median of mean estimates.

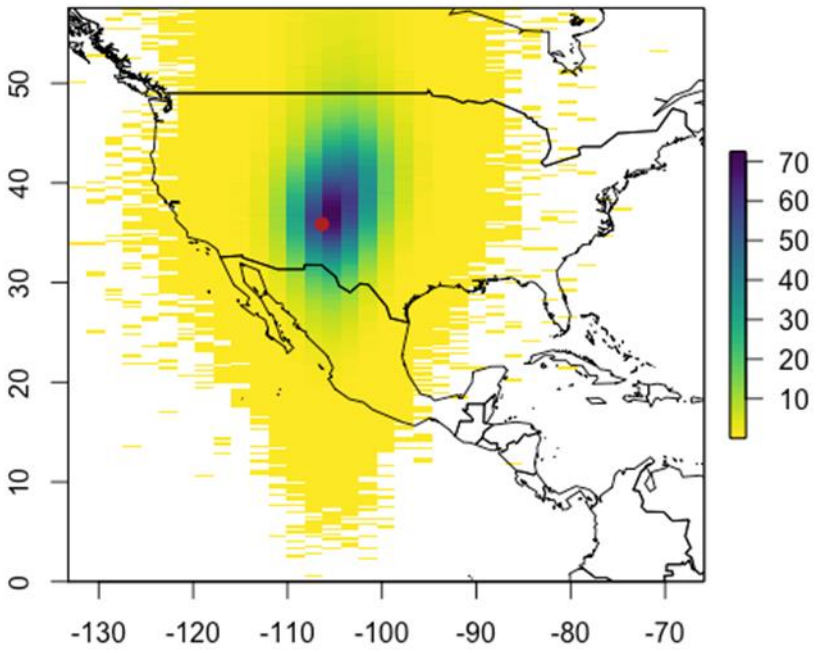

Figure D-11. SGAT-generated probability of location map for GLS unit 30, truncated to show area of highest probability estimates (see scale on left). Red circle shows deployment location.

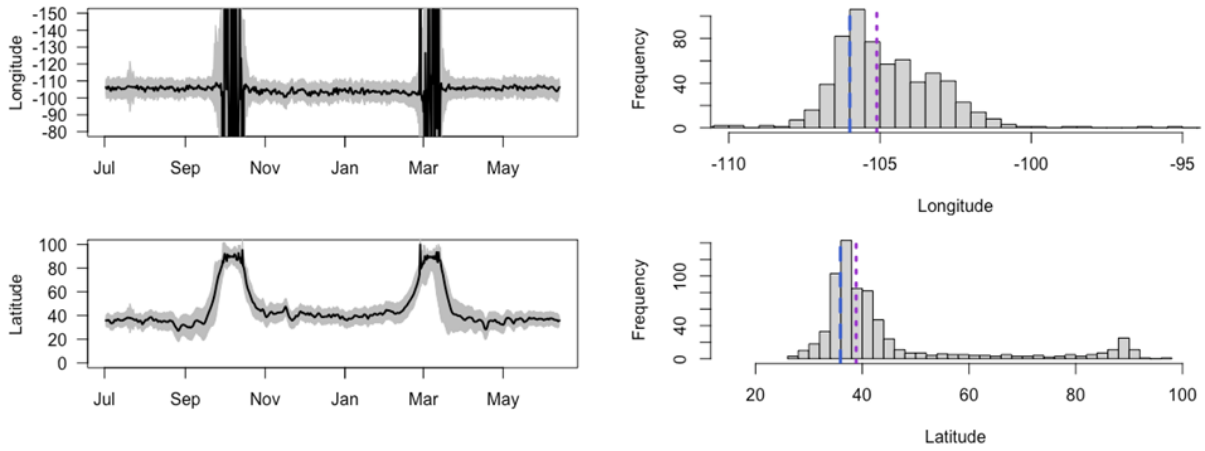

Figure D-12. Latitude and longitude estimates from SGAT analyses of GLS unit 30, truncated to show highest probability estimates. Left panel shows estimated latitude and longitude through time with gray 95% CI interval. Note extreme variation is expected around equinoxes. Right panel shows mean estimates from 10,000 iterations of SGAT model for longitude and latitude. Blue dashed lines show deployment locations; purple dashed lines show median of mean estimates.

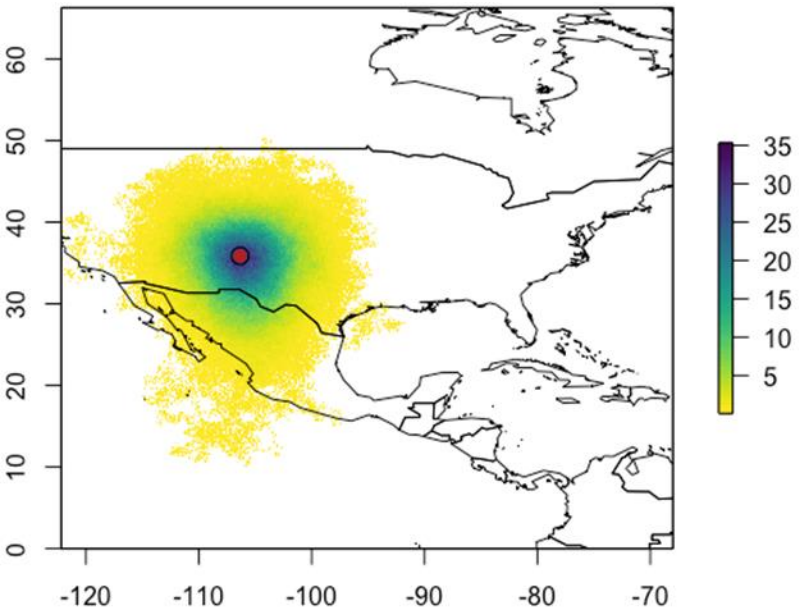

Figure D-13. SGAT-generated probability of location map for GLS unit 27, truncated to show area of highest probability estimates (see scale on left). Red circle shows deployment location. Note: Unable to tune SGAT models; presenting results from initial run of 10,000 iterations. Unable to extrapolate reasonable latitude or longitude through time estimates.

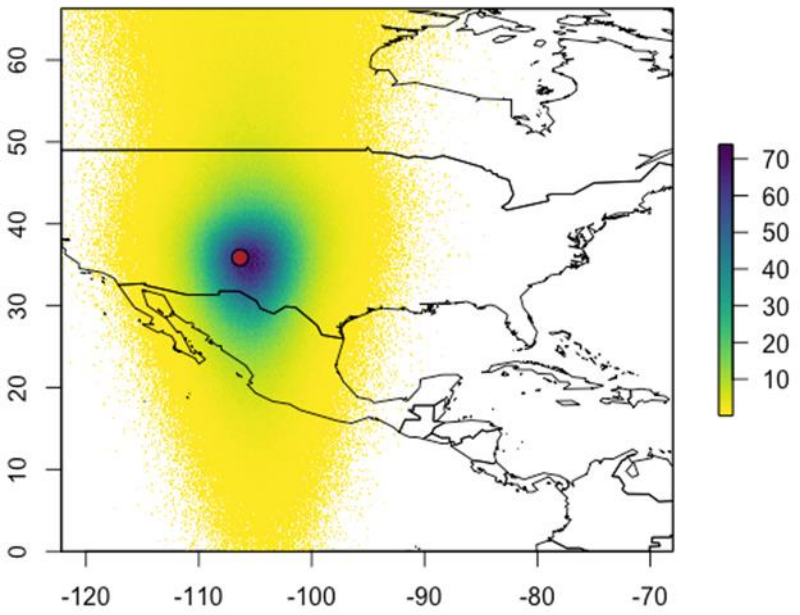

Figure D-14. SGAT-generated probability of location map for GLS unit 38, truncated to show area of highest probability estimates (see scale on left). Red circle shows deployment location.

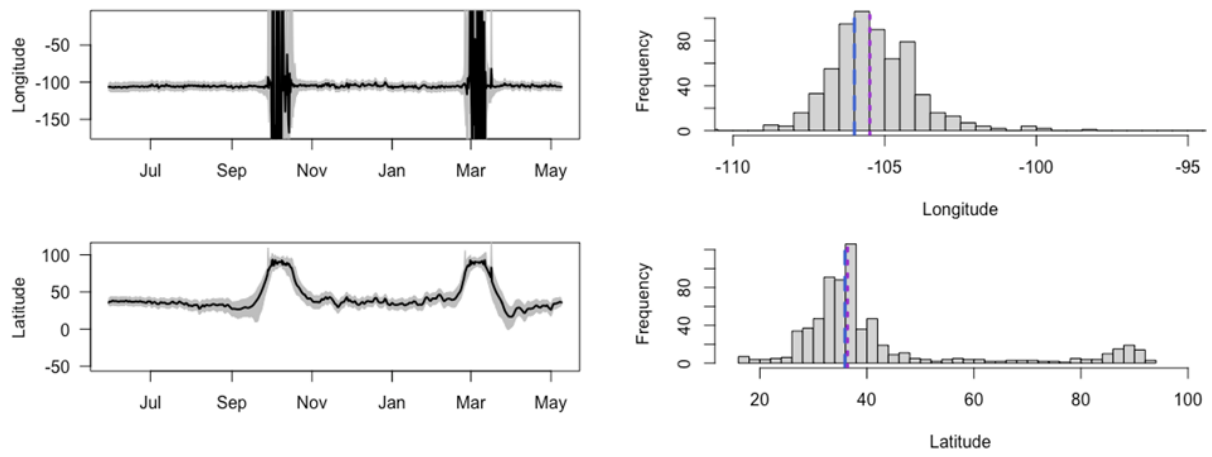

Figure D-15. Latitude and longitude estimates from SGAT analyses of GLS unit 38, truncated to show highest probability estimates. Left panel shows estimated latitude and longitude through time with gray 95% CI interval. Note extreme variation is expected around equinoxes. Right panel shows mean estimates from 10,000 iterations of SGAT model for longitude and latitude. Blue dashed lines show deployment locations; purple dashed lines show median of mean estimates.

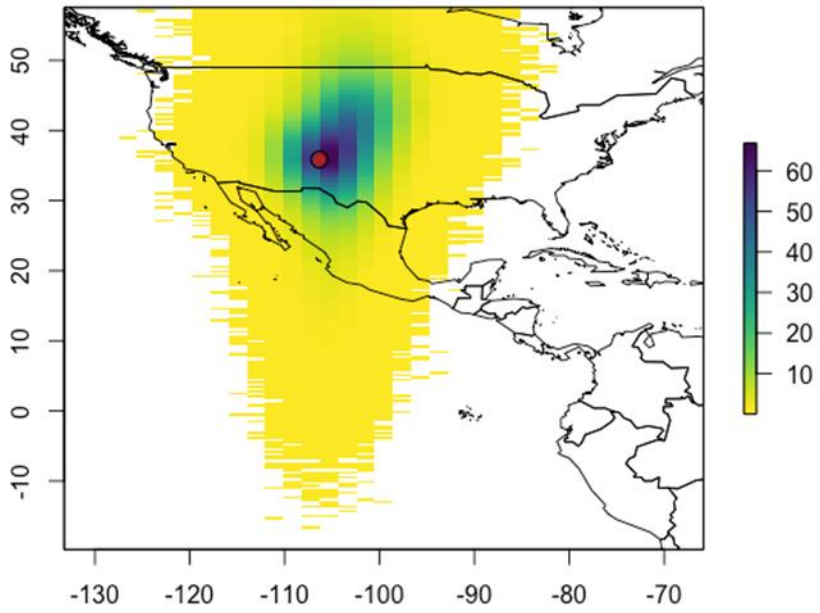

Figure D-16. SGAT-generated probability of location map for GLS unit 42, truncated to show area of highest probability estimates (see scale on left). Red circle shows deployment location.

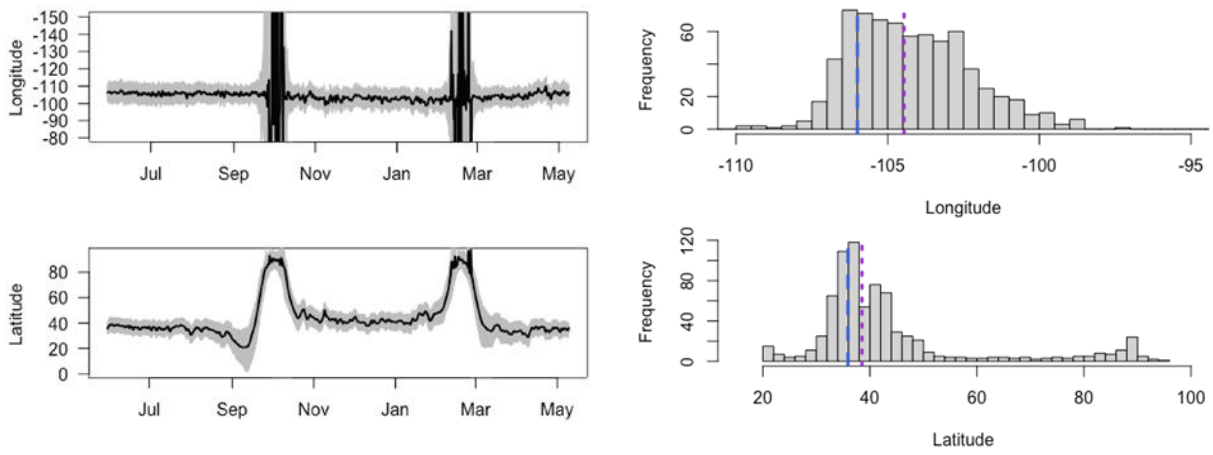

Figure D-17. Latitude and longitude estimates from SGAT analyses of GLS unit 42, truncated to show highest probability estimates. Left panel shows estimated latitude and longitude through time with gray 95% CI interval. Note extreme variation is expected around equinoxes. Right panel shows mean estimates from 10,000 iterations of SGAT model for longitude and latitude. Blue dashed lines show deployment locations; purple dashed lines show median of mean estimates.